

Theoretical studies of the dynamic structure function of liquid ^4He

E. Manousakis and V. R. Pandharipande

*Department of Physics and Materials Research Laboratory, University of Illinois at Urbana-Champaign,
1110 West Green Street, Urbana, Illinois 61801*

(Received 28 May 1985)

The dynamic structure factor $S(k, \omega)$ for liquid ^4He is studied with the use of perturbation theory in a correlated basis generated by the Feynman-Cohen (FC) excitation operator acting on the interacting ground state. We consider the coupling of one FC excitation to two FC excitations and sum the important contributions to all orders in perturbation theory. $S(k, \omega)$ is calculated for many values of k in the interval $(0.8 \text{ \AA}^{-1}, 4.5 \text{ \AA}^{-1})$. We find a low-energy δ -function peak which corresponds to the phonon-maxon-roton spectrum and report its energy $e(k)$ and $Z(k)$ as a function of k . "Two-quasiparticle" peaks are also found and they may be identified as roton-roton, maxon-maxon, and maxon-roton contributions. At high k , most of the strength of $S(k, \omega)$ is distributed in the neighborhood of quasifree scattering energy $\omega \simeq \hbar^2 k^2 / 2m$, and the results are comparable with results of the impulse approximation. Semiquantitative agreement is found between the calculated $S(k, \omega)$ and that inferred from neutron inelastic scattering experiments.

I. INTRODUCTION

Experimentally, the density fluctuations of liquid ^4He are studied by means of neutron inelastic scattering. In a linear-response regime the probability for scattering is proportional to the dynamic liquid structure function $S(k, \omega)$.

The measured $S(k, \omega)$ in the range of momentum transfers $0 < k \lesssim 2 \text{ \AA}^{-1}$ has a well-defined first peak, a broad structure at intermediate energies, and a high-energy tail. The first peak corresponds to one-quasiparticle excitation, and the intermediate-energy structure and the high-energy tail are attributed to multi-quasiparticle excitations. For very high momentum transfers the measured $S(k, \omega)$ has a broad peak in the vicinity of the free-particle energy $\hbar^2 k^2 / 2m$. At intermediate momentum transfers ($k \sim 2.5 \text{ \AA}^{-1}$), $S(k, \omega)$ has complex structure.

The origin, the energy dispersion curve $e(k)$, and the strength $Z(k)$ of the one-quasiparticle peak (first peak) are more or less understood.^{1,2}

There is evidence from Raman scattering experiments³ that in the long-wavelength limit there is a bound state of two paired rotons with opposite momenta. Zawadowski, Ruvalds, and Solana⁴ (ZRS) have suggested that the intermediate-energy structure of $S(k, \omega)$ may be explained by considering the excitation of roton-roton bound states. However, Svensson *et al.*⁵ find no indication that it is necessary to invoke the existence of two-roton bound states to explain the intermediate-energy structure in their neutron scattering data. In addition, Hasting and Halley⁶ have shown that no ZRS model can provide a quantitative account of the intermediate-energy structure of $S(k, \omega)$.

Jackson⁷ has studied $S(k, \omega)$ with microscopic theory, using a set of nonorthogonal correlated multiphonon states defined by

$$|n\rangle = \rho(\mathbf{k}_1)\rho(\mathbf{k}_2) \cdots \rho(\mathbf{k}_n)|0\rangle, \quad (1.1)$$

Where $\rho(\mathbf{k})$ is the \mathbf{k} Fourier transform of the density operator and $|0\rangle$ is the ground state. He considered the one- and two-phonon contribution to $S(k, \omega)$, calculated the one-particle Green's function in perturbation theory, and related the spectral function to $S(k, \omega)$. In this calculation the peaks of $S(k, \omega)$ appear at much higher energies than do the experimental ones.

The interplay between the one-quasiparticle and two-quasiparticle contributions to $S(k, \omega)$ has also been examined⁸ using its various ω moments. Within the framework of this approach, using the sum rules, one can place constraints on the multi-quasiparticle contribution.

Recently we studied² the one-quasiparticle excitations in liquid ^4He using perturbation theory in the Feynman-Cohen⁹ (FC) basis. A nonorthogonal set of correlated basis functions (CBF's) is generated by the FC excitation operator:

$$\rho_B(\mathbf{k}) \equiv \sum_{i=1}^N e^{i\mathbf{k}\cdot\mathbf{r}_i} \left[1 + i \sum_{j \neq i}^N \mathbf{k}\cdot\mathbf{r}_{ij} \eta(r_{ij}) \right]. \quad (1.2)$$

$\eta(r)$ is the backflow velocity potential determined in Ref. 2 by means of variational calculations. The CBF n -quasiparticle state is defined as

$$|n\rangle \equiv \rho_B(\mathbf{k}_1)\rho_B(\mathbf{k}_2) \cdots \rho_B(\mathbf{k}_n)|0\rangle. \quad (1.3)$$

The diagonal elements of the Hamiltonian matrix in this basis constitute the unperturbed part H_0 and the off-diagonal elements form the perturbation H_I . The zeroth order (unperturbed) one-quasiparticle states and energies are the FC variational results. In Ref. 2 we carried out a detailed variational calculation of the one-quasiparticle spectrum using the FC ansatz in conjunction with the hypernetted-chain (HNC) technique. We found that the FC states are accurate for the phonons but the maxon and roton energies are $\sim 20\%$ too high. We calculated the second-order corrections due to the coupling of one-FC-quasiparticle state to two-FC-quasiparticle states. These

corrections improve the agreement with the experiment significantly; the theoretical $e(k)$ is within 5% of the experimental spectrum and the calculated strength $Z(k)$ is within $\sim 30\%$ of the experimental strength.

In this paper we calculate the one- and two-quasiparticle contribution to $S(k, \omega)$. A perturbative expansion of the density correlation function is developed in the correlated basis (1.3). We consider only the coupling of one FC excitation to two FC excitations and sum the important contributions to all orders in perturbation theory. The $S(k, \omega)$ is trivially obtained from the density correlation function.

We calculate $S(k, \omega)$ for k in the interval (0.8 \AA^{-1} , 4.5 \AA^{-1}) and find that the one-quasiparticle excitation is well defined at all values of k . It exhausts more than half of the strength of $S(k, \omega)$ for $0 < k \lesssim 2 \text{ \AA}^{-1}$; however, its strength $Z(k)$ becomes very small for k greater than 3 \AA^{-1} . We also find smaller peaks at intermediate energies that can be identified as simultaneous excitations of two rotons or two maxons and one maxon plus one roton. For $2 \text{ \AA}^{-1} \lesssim k \lesssim 3 \text{ \AA}^{-1}$, a two-peak structure is found for $S(k, \omega)$; the first peak is the continuation of the "one-quasiparticle" branch, while the second is close to the Feynman-phonon energy of $\hbar^2 k^2 / 2mS(k)$. For $k \gtrsim 3 \text{ \AA}^{-1}$ most of the strength is distributed in the neighborhood of $\hbar^2 k^2 / 2m$. For $k > 4 \text{ \AA}^{-1}$ the calculated $S(k, \omega)$ is comparable to that obtained using the momentum distribution and the impulse approximation. The main

features of the experimental $S(k, \omega)$, over a wide range of k and ω , are semiquantitatively explained by this microscopic theory.

The theoretical calculation of the density correlation and dynamic liquid structure functions using CBF perturbation theory is discussed in Sec. II, and the results are given in Sec. III.

II. THEORY

The density correlation function is defined as

$$D(k, \omega) \equiv \left\langle 0 \left| \rho_{\mathbf{k}}^\dagger \frac{1}{H - E_0 - \omega - i\eta} \rho_{\mathbf{k}} \right| 0 \right\rangle, \quad (2.1)$$

where E_0 is the ground-state energy and we take the limit $\eta \rightarrow 0$. It is known¹⁰ that

$$S(k, \omega) = \frac{1}{\pi} \text{Im}[D(k, \omega)]. \quad (2.2)$$

We write the many-body Hamiltonian H as

$$H = H_0 + H_I, \quad (2.3)$$

where

$$\langle n | H_0 | m \rangle \equiv \delta_{nm} \langle n | H | n \rangle, \quad (2.4)$$

$$\langle n | H_I | m \rangle \equiv (1 - \delta_{nm}) \langle n | H | m \rangle, \quad (2.5)$$

and $|m\rangle, |n\rangle, \dots$ are orthonormalized FC states (1.3). On performing a Goldstone-type perturbative expansion for $D(k, \omega)$ we obtain

$$D(k, \omega) = \sum_{n \neq 0} (-1)^n \left\langle 0 \left| \rho_{\mathbf{k}}^\dagger \frac{1}{H_0 - E_0 - \omega - i\eta} \left[H_I \frac{1}{H_0 - E_0 - \omega - i\eta} \right]^n \rho_{\mathbf{k}} \right| 0 \right\rangle. \quad (2.6)$$

For the moment, we allow only for one- or two-FC-quasiparticle intermediate states $|\mathbf{k}\rangle$ and $|l, \mathbf{m}\rangle$. These are obtained by orthonormalizing the following FC states:

$$|1\rangle = \rho_B(\mathbf{k}) |0\rangle, \quad (2.7)$$

$$|2\rangle = \rho_B(l) \rho_B(\mathbf{m}) |0\rangle, \quad (2.8)$$

$$|\mathbf{k}\rangle = |1\rangle / (N_{11})^{1/2}, \quad (2.9)$$

$$|l, \mathbf{m}\rangle = \left[|2\rangle - \frac{N_{12}}{N_{11}} |1\rangle \right] / (N_{22})^{1/2}, \quad (2.10)$$

$$N_{ij} \equiv \langle i | j \rangle. \quad (2.11)$$

The coupling of one-FC-quasiparticle to two-FC-quasiparticle states is real and is defined as

$$a(k, l, m) \equiv \langle \mathbf{k} | H - E_0 | l, \mathbf{m} \rangle = \langle l, \mathbf{m} | H - E_0 | \mathbf{k} \rangle. \quad (2.12)$$

The terms of the series (2.6) are represented by diagrams such as those of Figs. 1(a) and 1(b). A single line labeled \vec{k} denotes a one-FC-quasiparticle propagator:

$$G_1^{(0)}(k, \omega) = \frac{1}{e_B(k) - \omega - i\eta}, \quad (2.13)$$

where $e_B(k)$ is the FC one-quasiparticle energy, i.e.,

$$e_B(k) \equiv \langle \mathbf{k} | H - E_0 | \mathbf{k} \rangle, \quad (2.14)$$

and a double line labeled \vec{l}, \vec{m} denotes the propagator of the two-FC-quasiparticle state

$$G_2^{(0)}(l, m, \omega) \equiv \frac{1}{e_B(l) + e_B(m) - \omega - i\eta}. \quad (2.15)$$

The vertices are given in Figs. 1(c)–1(e). We define

$$\xi_1(k) \equiv \langle 0 | \rho_{\mathbf{k}}^\dagger | \mathbf{k} \rangle = \langle \mathbf{k} | \rho_{\mathbf{k}} | 0 \rangle, \quad (2.16)$$

and

$$\xi_2(k, l, m) \equiv \langle 0 | \rho_{\mathbf{k}}^\dagger | l, \mathbf{m} \rangle = \langle l, \mathbf{m} | \rho_{\mathbf{k}} | 0 \rangle. \quad (2.17)$$

Note that both ξ_1 and ξ_2 are real. In this notation, for example, the contribution of Fig. 1(a) is given by

$$\xi_1(k) G_1^{(0)}(k, \omega) a(k, l, m) G_2^{(0)}(l, m, \omega) \xi_2(k, l, m), \quad (2.18)$$

and a summation over the two-quasiparticle momenta l, \mathbf{m}

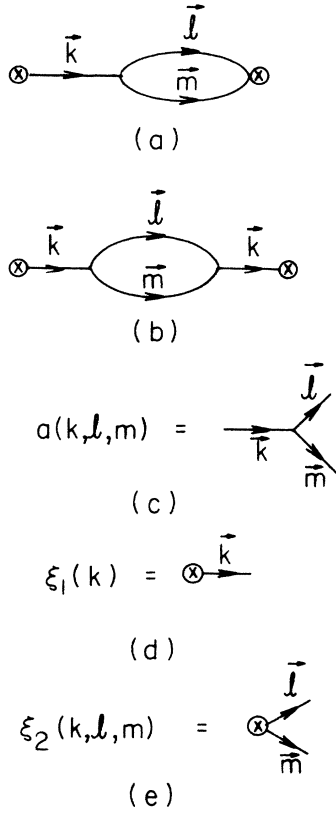


FIG. 1. Diagrammatic representation of terms appearing in $D(k, \omega)$ [Eq. (2.6)].

is assumed. We can have the following three types of terms.

(i) First, there are terms having $\langle 0 | \rho_{\mathbf{k}}^\dagger | \mathbf{k} \rangle$ on the left and $\langle \mathbf{k} | \rho_{\mathbf{k}} | 0 \rangle$ on the right. The contribution of such terms is denoted by $D_{11}(k, \omega)$, and it is the sum of the terms in Fig. 2(a). We obtain

$$D_{11}(k, \omega) = \frac{\xi_1^2(k)}{e_B(k) + \Sigma_0(k, \omega) - \omega - i\eta}, \quad (2.19)$$

where

$$\Sigma_0(k, \omega) = -\frac{1}{2} \sum_{l, m} |a(k, l, m)|^2 G_2^{(0)}(l, m, \omega). \quad (2.20)$$

Here, we define $\Sigma_0(k, \omega)$ as the self-energy insertion (2.20); we reserve the notation $\Sigma(k, \omega)$ for the next, improved approximation.

(ii) Second, terms having $\langle 0 | \rho_{\mathbf{k}}^\dagger | \mathbf{k} \rangle$ on the left and $\langle l, m | \rho_{\mathbf{k}} | 0 \rangle$ on the right [Fig. 2(b)] and vice versa [Fig. 2(c)] are denoted by $D_{12}(k, \omega)$ and $D_{21}(k, \omega)$, respectively. Their contribution is given by

$$D_{12}(k, \omega) = \frac{\xi_1(k)\theta(k, \omega)}{e_B(k) + \Sigma_0(k, \omega) - \omega - i\eta}, \quad (2.21)$$

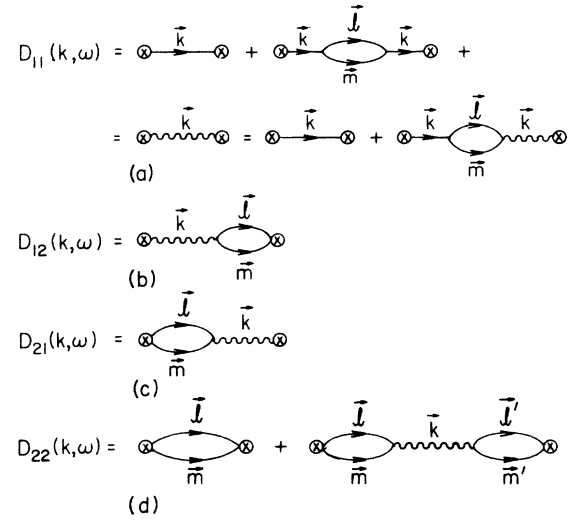


FIG. 2. Various contributions to $D(k, \omega)$.

where

$$\theta(k, \omega) = -\frac{1}{2} \sum_{l, m} \xi_2(k, l, m) G_2^{(0)}(l, m, \omega) a(k, l, m), \quad (2.22)$$

and

$$D_{21}(k, \omega) = D_{12}(k, \omega). \quad (2.23)$$

(iii) Finally we have the terms of Fig. 2(d) with $\langle 0 | \rho_{\mathbf{k}}^\dagger | l, m \rangle$ on the left and $\langle l', m' | \rho_{\mathbf{k}} | 0 \rangle$ on the right. Their contribution is given by

$$D_{22}(k, \omega) = \frac{1}{2} \sum_{l, m} |\xi_2(k, l, m)|^2 G_2^{(0)}(l, m, \omega) + \frac{\theta^2(k, \omega)}{e_B(k) + \Sigma_0(k, \omega) - \omega - i\eta}. \quad (2.24)$$

In this approximation

$$D(k, \omega) = D_{11}(k, \omega) + 2D_{12}(k, \omega) + D_{22}(k, \omega), \quad (2.25)$$

and we can combine the ξ_1^2 , $2\xi_1\theta$, and θ^2 terms to obtain

$$D(k, \omega) = \frac{[\xi_0(k, \omega)]^2}{e_B(k) + \Sigma_0(k, \omega) - \omega - i\eta} + D'_0(k, \omega), \quad (2.26)$$

where

$$\xi_0(k, \omega) \equiv \xi_1(k) + \theta(k, \omega) \quad (2.27)$$

and

$$D'_0(k, \omega) = \frac{1}{2} \sum_{l, m} |\xi_2(k, l, m)|^2 G_2^{(0)}(l, m, \omega). \quad (2.28)$$

By using Eq. (2.2) the dynamic structure function is simply given by

$$S(k, \omega) = \pi^{-1} [2 \operatorname{Re}[\xi_0(k, \omega)] \operatorname{Im}[\xi_0(k, \omega)] \{e_B(k) + \operatorname{Re}[\Sigma_0(k, \omega)] - \omega\} - \operatorname{Im}[\Sigma_0(k, \omega)] \{ \operatorname{Re}[\xi_0(k, \omega)] \}^2 - \{ \operatorname{Im}[\xi_0(k, \omega)] \}^2] \times \{ [e_B(k) + \operatorname{Re}[\Sigma_0(k, \omega)] - \omega]^2 + \{ \operatorname{Im}[\Sigma_0(k, \omega)] \}^2 \}^{-1} + \operatorname{Im}[D'_0(k, \omega)], \quad (2.29)$$

where

$$\text{Re}[\xi_0(k, \omega)] = \xi_1(k) - \frac{1}{2} \sum_{l, m} \xi_2(k, l, m) a(k, l, m) \text{Re}[G_2^{(0)}(l, m, \omega)], \quad (2.30)$$

$$\text{Im}[\xi_0(k, \omega)] = -\frac{1}{2} \sum_{l, m} \xi_2(k, l, m) a(k, l, m) \text{Im}[G_2^{(0)}(l, m, \omega)]. \quad (2.31)$$

Similarly, in calculating the real and imaginary parts of $\Sigma_0(k, \omega)$ and $D'_0(k, \omega)$ we take the real and imaginary part of $G_2^{(0)}(l, m, \omega)$ inside the sums of Eqs. (2.20) and (2.28), respectively. Here

$$\text{Re}[G_2^{(0)}(l, m, \omega)] = P \frac{1}{e_B(l) + e_B(m) - \omega}, \quad (2.32)$$

$$\text{Im}[G_2^{(0)}(l, m, \omega)] = \pi \delta(\omega - e_B(l) - e_B(m)). \quad (2.33)$$

The symbol P stands for the Cauchy principal value. In this approximation the one-quasiparticle pole of $D(k, \omega)$ is at $\omega = e(k)$ given by

$$e(k) = e_B(k) + \Sigma_0(k, e(k)), \quad (2.34)$$

and if the $\text{Im}[\Sigma_0(k, \omega)] = 0$ and $\text{Im}[\xi_0(k, \omega)] = 0$, the residue of the pole is

$$Z(k) = \left[\frac{\xi_0^2(k, \omega)}{1 - \frac{\partial \Sigma_0(k, \omega)}{\partial \omega}} \right]_{\omega=e(k)}, \quad (2.35)$$

and the contribution from the pole to $S(k, \omega)$ is $Z(k)\delta(\omega - e(k))$.

We note that the expression (2.34) for $e(k)$ is the Brillouin-Wigner perturbation formula used in Ref. 2. Moreover, the expression (2.35) is also identical to the ex-

pression for the $Z(k)$ used in Ref. 2; namely,

$$Z(k) = \frac{|\langle 0 | \rho_{\mathbf{k}}^\dagger | \psi(\mathbf{k}) \rangle|^2}{\langle \psi(\mathbf{k}) | \psi(\mathbf{k}) \rangle}, \quad (2.36)$$

where $\psi(\mathbf{k})$ is the perturbed one-quasiparticle state given by

$$|\psi(\mathbf{k})\rangle = |\mathbf{k}\rangle - \frac{1}{2} \sum_{l, m} a(k, l, m) G_2^{(0)}(l, m, \omega) |l, m\rangle. \quad (2.37)$$

Notice that the denominator of (2.35) is identically equal to the norm of $\psi(\mathbf{k})$.

In this calculation, the results for the one-quasiparticle contribution are identical to those of Ref. 2. In Ref. 2 we have seen that the differences between the variational (FC) and the experimental one-quasiparticle spectrum are essentially removed by the inclusion of the second-order correction given by Eq. (2.34). However, this approximation does not describe well the two-quasiparticle contribution to $S(k, \omega)$, because the two-quasiparticle propagator [Eq. (2.15)] has poles at the FC energies. This is a consequence of our approximation to include only one- and two-FC-quasiparticle intermediate states. To obtain the two-quasiparticle contribution at reasonable energies we must consider self-energy insertions in the propagation of the double lines. On including some of the simpler self-energy insertions shown in Fig. 3, the two-quasiparticle propagator is modified as

$$G_2(l, m, \omega) = \frac{1}{e_B(l) + \Sigma_0(l, \omega - e_B(m)) + e_B(m) + \Sigma_0(m, \omega - e_B(l)) - \omega - i\eta}, \quad (2.38)$$

and, hence, the quantities $\Sigma_0(k, \omega)$, $\xi_0(k, \omega)$, and $D'_0(k, \omega)$ entering in the expression for $D(k, \omega)$ [Eq. (2.26)] are, respectively, modified as

$$\Sigma(k, \omega) = -\frac{1}{2} \sum_{l, m} |a(k, l, m)|^2 G_2(l, m, \omega), \quad (2.39)$$

$$\xi(k, \omega) = \xi_1(k) - \frac{1}{2} \sum_{l, m} \xi_2(k, l, m) G_2(l, m, \omega) a(k, l, m), \quad (2.40)$$

$$D'(k, \omega) = \frac{1}{2} \sum_{l, m} |\xi_2(k, l, m)|^2 G_2(l, m, \omega). \quad (2.41)$$

$S(k, \omega)$ in this approximation is still given by Eq. (2.29) by replacing the real and imaginary part of $\Sigma_0(k, \omega)$, $\xi_0(k, \omega)$, and $D'(k, \omega)$ by those of Eqs. (2.39)–(2.41). The

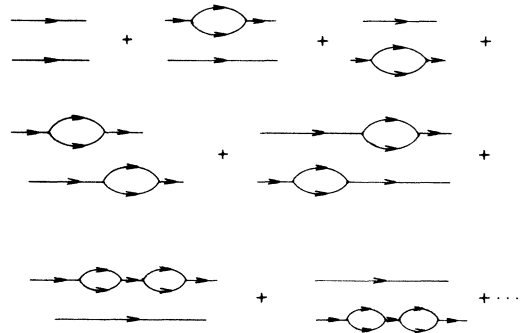


FIG. 3. Self-energy insertions in the two-quasiparticle propagator G_2 .

real and imaginary parts of the above quantities come from the real and imaginary parts of $G_2(l, m, \omega)$ given by

$$\text{Re}[G_2(l, m, \omega)] = \frac{e_2(l, m, \omega) - \omega}{[e_2(l, m, \omega) - \omega]^2 + \Gamma_2^2(l, m, \omega)}, \quad (2.42)$$

$$\text{Im}[G_2(l, m, \omega)] = -\frac{\Gamma_2(l, m, \omega)}{[e_2(l, m, \omega) - \omega]^2 + \Gamma_2^2(l, m, \omega)}, \quad (2.43)$$

where

$$e_2(l, m, \omega) = e_B(l) + \text{Re}[\Sigma_0(l, \omega - e_B(m))] + e_B(m) + \text{Re}[\Sigma_0(m, \omega - e_B(l))], \quad (2.44)$$

$$\Gamma_2(l, m, \omega) = \text{Im}[\Sigma_0(l, \omega - e_B(m))] + \text{Im}[\Sigma_0(m, \omega - e_B(l))]. \quad (2.45)$$

If $\Gamma_2(l, m, \omega) = 0$, then of course

$$\text{Re}[G_2(l, m, \omega)] = P \frac{1}{e_2(l, m, \omega) - \omega}, \quad (2.46)$$

$$\text{Im}[G_2(l, m, \omega)] = \pi \delta(\omega - e_2(l, m, \omega)). \quad (2.47)$$

To calculate $S(k, \omega)$ we need the matrix elements (i) of the Hamiltonian, i.e., $e_B(k)$ and $a(k, l, m)$, (ii) of the unit operator, i.e., N_{ij} , and (iii) of the density operator, i.e., $\langle 0 | \rho_k^\dagger | 1 \rangle$ and $\langle 0 | \rho_k^\dagger | 2 \rangle$. All of them have been calculated in Ref. 2 and we use them here.

The numerical calculation of the real and imaginary parts of the quantities entering in the expression of $S(k, \omega)$ is explained in the Appendix.

III. RESULTS AND DISCUSSION

Using the two-particle propagator with the self-energy insertions, we have calculated $S(k, \omega)$ for various values of k in the interval $0.8 \text{ \AA}^{-1} < k < 4.5 \text{ \AA}^{-1}$. For smaller values of k the total strength of $S(k, \omega)$ is almost exhausted by the one-phonon peak at energy $e(k) = \hbar ck$ and strength $Z(k) - S(k) = (\hbar/2mc)k$, where c is the sound velocity. In general we find the following three different kinds of peaks in $S(k, \omega)$.

(i) There is a well-defined δ function peak at energy $e(k)$ for all values of k in the above interval. $S(k, \omega < e(k))$ is zero. This peak corresponds to the excitation of one quasiparticle out of the condensate. Its dispersion $e(k)$ gives the phonon-maxon-roton-endon spectrum (the excitations at $k \geq 2.4 \text{ \AA}^{-1}$ are often called endons). The strength $Z(k)$ of this peak becomes very small for large k ($> 3 \text{ \AA}^{-1}$).

(ii) There are peaks which presumably can be identified as a result of simultaneous excitation of two quasiparticles.

(iii) At high k we find that the main peak in the calculated $S(k, \omega)$ is a somewhat broad peak in the vicinity of $\hbar^2 k^2 / 2m$ as may be expected from the impulse approximation and sum rules. We call this peak the quasifree peak.

On the other hand we divide the range of k into the following three regions.

(i) The region of $k \lesssim 2.2 \text{ \AA}^{-1}$, where the main peak is the one-quasiparticle peak and peaks of secondary importance are the two-quasiparticle excitations.

(ii) The region $k \geq 2.7 \text{ \AA}^{-1}$, where the main peak is the "quasifree" peak and there are other secondary peaks of two-quasiparticle excitations at lower energies.

(iii) In the narrow interval $2.2 \text{ \AA}^{-1} \lesssim k \leq 2.7 \text{ \AA}^{-1}$ the strength of the one-quasiparticle peak decreases very fast, while that in the quasifree region increases. At $k = 2.5 \text{ \AA}^{-1}$ we have two peaks of comparable strength; the low-energy one is on the continuation of the phonon-maxon-roton curve, while that at high ω is close to the quasifree.

A. The one-quasiparticle peak

The $D(k, \omega)$ has a pole at $\omega = e(k)$ where the $\text{Im}[\Sigma(k, e(k))] = 0$. This gives the so-called one-quasiparticle contribution $Z(k)\delta(\omega - e(k))$ to $S(k, \omega)$. The $e(k)$ is obtained by solving the Eq. (2.34) with the full Σ instead of the Σ_0 , and the $Z(k)$ from Eq. (2.35) with ξ and Σ instead of ξ_0 and Σ_0 . The calculated energies $e(k)$ for the values of $k < 3.0 \text{ \AA}^{-1}$ are shown by the + signs in Fig. 4. The open circles are the experimental data and the solid line (from Ref. 2) is obtained by solving Eq. (2.34) using Σ_0 . Figure 5 presents the calculated $Z(k < 3.0 \text{ \AA}^{-1})$. [+ signs for the full calculation, solid curve (from Ref. 2) for calculation with ξ_0 and Σ_0 , and the dashed curve for the experimental data¹¹.] We see from Figs. 4 and 5 that the effect of the self-energy inser-

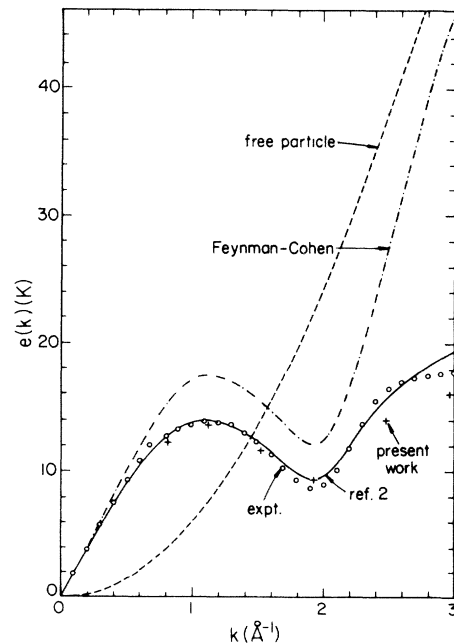


FIG. 4. The one-quasiparticle spectrum. The dashed line is the free-particle spectrum $\hbar^2 k^2 / 2m$ and the dashed-dotted line is the Feynman-Cohen variational spectrum. The solid line and + signs represent the $e(k)$ obtained with Σ_0 and Σ , respectively, and the \circ 's show experimental data (Ref. 11).

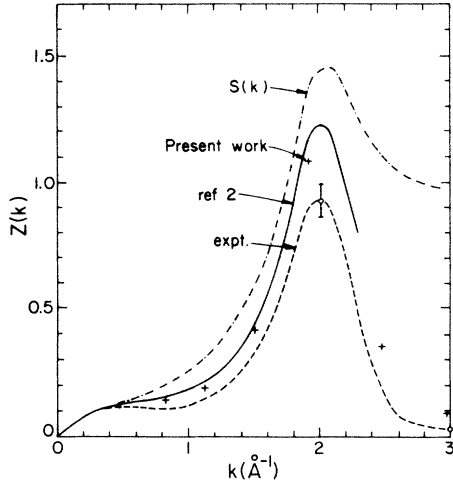


FIG. 5. The strength $Z(k)$. The solid line and + signs give the results of calculations with $G_2^{(0)}$ and G_2 respectively. The dashed and dashed-dotted lines are the experimental $Z(k)$ and $S(k)$, respectively.

tions in G_2 is not too significant for the one-quasiparticle contribution.

The total strength of $S(k, \omega)$ is given by $S(k)$:

$$\int d\omega S(k, \omega) = S(k). \quad (3.1)$$

The contribution to the above sum rule from the one-quasiparticle excitation is $Z(k)$; the rest, $S(k) - Z(k)$, comes from two or more quasiparticle contributions. $S(k)$ is also plotted in Fig. 5 (dashed-dotted curve). We can see from this figure that in the range $k \lesssim 2.3 \text{ \AA}^{-1}$ the one-quasiparticle excitation gives the major contribution to $S(k, \omega)$. For $k \gtrsim 2.5 \text{ \AA}^{-1}$, however, the contribution of this excitation is relatively small.

The f sum rule

$$\int d\omega \omega S(k, \omega) = \frac{\hbar^2 k^2}{2m}, \quad (3.2)$$

is satisfied by the exact $S(k, \omega)$. The one-quasiparticle contribution to it is given by $Z(k)e(k)$. If one assumes that the one-quasiparticle contribution exhausts the sum rules (3.1) and (3.2), then $Z(k) = S(k)$ and $e(k)$ is given by the Bijl-Feynman energy $\hbar^2 k^2 / 2mS(k)$.

B. Two-quasiparticle peaks

We find several peaks which may be identified as two-quasiparticle excitations. These never become the major structures of $S(k, \omega)$. For $0.8 \text{ \AA}^{-1} \leq k \leq 2.0 \text{ \AA}^{-1}$ they provide intermediate-energy structure in the range $14 \text{ K} \lesssim \omega \lesssim 30 \text{ K}$; and contribute 10–20% of the overall strength. The results are shown in Figs. 6–9. The vertical lines in these figures show the one-quasiparticle δ -function contribution. The strength $Z(k)$ is given in a box on the line. The strength of the rest of the contribution is given in a box under the two-quasiparticle peaks, and the total strength $S(k)$ is given along with the value of k in the top right-hand corner. The results of our calculations with the $G_2^{(0)}$ are shown by dashed lines in Figs. 6 and 7. We note that as expected the self-energy inser-

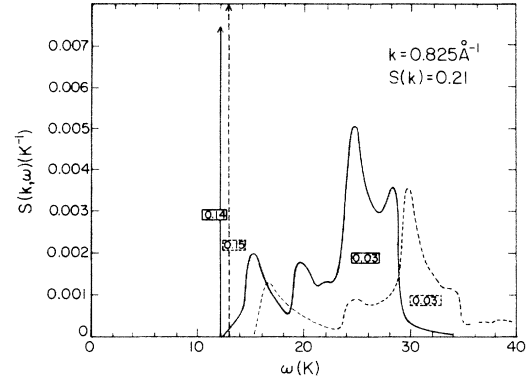


FIG. 6. The $S(k=0.825 \text{ \AA}^{-1}, \omega)$. The dashed and solid lines correspond to the calculations with $G_2^{(0)}$ and G_2 , respectively. The numbers in boxes give the strengths of the δ function, and the two-quasiparticle contribution to $S(k, \omega)$. The values of k and $S(k)$ are given in the top-right corner.

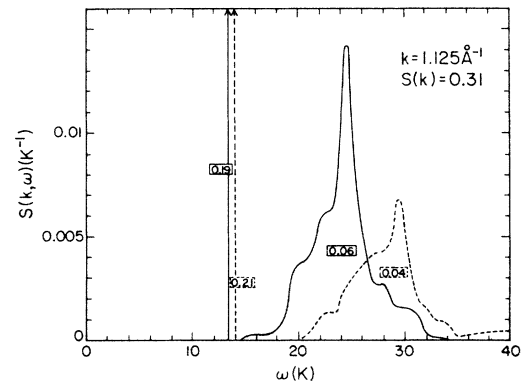


FIG. 7. The $S(k=1.125 \text{ \AA}^{-1}, \omega)$; see caption of Fig. 6 for details.

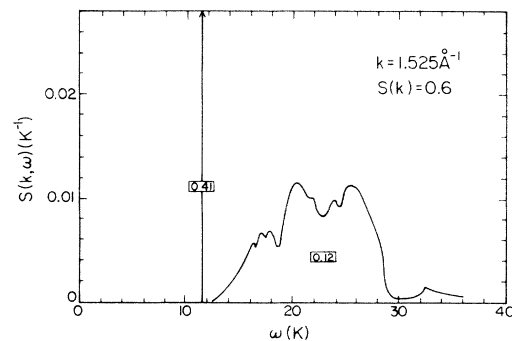


FIG. 8. The $S(k=1.525 \text{ \AA}^{-1}, \omega)$; see caption of Fig. 6 for details.

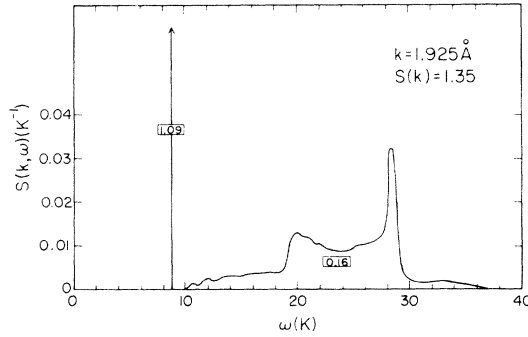


FIG. 9. The $S(k=1.925 \text{ \AA}^{-1}, \omega)$; see caption of Fig. 6 for details.

tions in G_2 have a significant effect on the energies of the two-quasiparticle peaks.

In order to understand the origin of the various peaks in this interval, we study the two-quasiparticle density of states (DOS) defined as

$$\rho_2(k, \omega) = \frac{1}{N} \frac{1}{2} \sum_{l, m} \delta_{\mathbf{k}, l+m} \delta(\omega - e(l) - e(m)). \quad (3.3)$$

It is instructive to understand the structure of the DOS. The one-quasiparticle DOS diverges at the roton minimum and maxon maximum. Therefore, we expect that combinations of the above extrema to give large contributions to the two-quasiparticle DOS and study them in detail.

a. Two rotons. We consider two rotons on the roton sphere as shown in Fig. 10(a) with center of mass momentum $\mathbf{k} = l + m$ ($|l| = |m| = k_r$, k_r is the location of the roton minimum) and total energy $\omega = 2\omega_r$, where ω_r denotes the roton energy. As long as k remains finite ($\neq 0$) there is only one angle θ for which $\mathbf{k} = l + m$; namely, that with $\cos\theta = \hat{\mathbf{k}} \cdot \hat{l} = k/2k_r$. If $k=0$, θ can take any

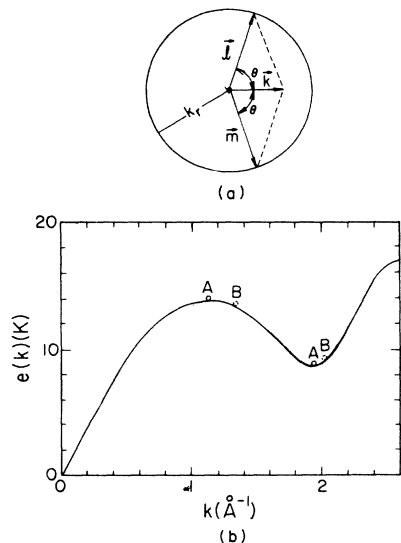


FIG. 10. (a) \vec{l} and \vec{m} are the momenta of the two-particles on the roton sphere and \vec{k} is their total momentum. (b) The two two-quasiparticle states A and B that have the same energy.

value from 0 to π . In this case, $\rho_2(k, \omega)$ diverges. In the case $k \neq 0$ ($k < 2k_r$), however, the phase space is limited and the two-roton DOS is finite at $\omega = 2\omega_r$.

b. Two maxons. The analysis here is identical to the two-roton case, i.e., for $k=0$ there is a singularity at $\omega = 2\omega_m$, where ω_m is the maxon energy, but for $k \neq 0$ ($k < 2k_m$; k_m is the maxon momentum) the DOS at $\omega = 2\omega_m$ is finite.

c. One maxon plus one roton. If $k_r - k_m < k < k_r + k_m$ (i.e., $0.8 \text{ \AA}^{-1} \lesssim k \lesssim 3 \text{ \AA}^{-1}$), a simultaneous excitation of one roton and one maxon can contribute to the two-quasiparticle DOS in the vicinity of $\omega = \omega_r + \omega_m$. There are a lot of degenerate states which have the above energy. We can demonstrate this as follows. We put a particle at the roton minimum and another at the maxon peak, so we create the state $|A\rangle = |k_r, k_m\rangle$. Next we move the first particle a little away from the roton minimum and at the same time we let the maxon move to a neighboring state so that the energy of the new two-particle state B [Fig. 10(b)] is the same as that of the state A . If $k_r - k_m < k < k_r + k_m$, we can always choose the directions of the momenta of the new state to satisfy the momentum conservation. Hence, there is a large (ultimately infinite) number of two-quasiparticle states in the neighborhood of $\omega = \omega_r + \omega_m$. In fact, if one approximates the spectrum in the vicinity of the roton and maxon by two parabolas, it is easy to show that there is a logarithmic singularity in the two-quasiparticle DOS for $\omega \sim \omega_r + \omega_m$:

$$\rho_2(k, \omega) \propto -\ln |\omega - \omega_r - \omega_m|. \quad (3.4)$$

The results of the numerically calculated DOS are shown in Fig. 11. We used the experimental dispersion curve with a momentum cutoff such that l and m are both less than 2.4 \AA^{-1} [$e(2.4 \text{ \AA}^{-1}) = 15.5 \text{ K}$]. The inclusion of states with higher momenta (greater than 2.4 \AA^{-1}) does not modify the $\rho_2(k, \omega)$ for $\omega \leq 24 \text{ K}$, but it will of course alter the DOS for higher ω . We can see that the main peak is at the maxon plus roton energy $\omega \simeq 22.5 \text{ K}$.

In Fig. 12 we present the matrix elements

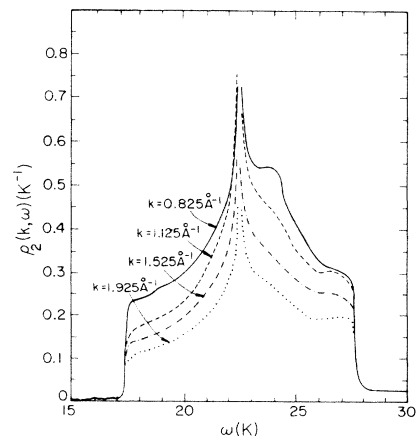


FIG. 11. Two-quasiparticle density of states at various values of k .

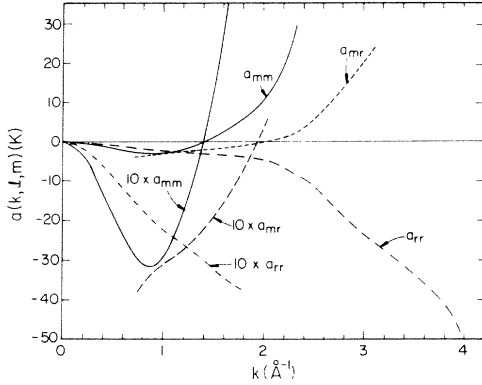


FIG. 12. The matrix element $a(k, l, m)$ when l and m are both maxons (a_{mm}), both rotons (a_{rr}), and a maxon and a roton (a_{mr}), as a function of k .

$$a_{rr}(k) = a(k, |l| = k_r, |m| = k_r),$$

$$a_{mm}(k) = a(k, |l| = k_m, |m| = k_m),$$

and

$$a_{mr}(k) = a(k, |l| = k_m, |m| = k_r)$$

for the cases of roton-roton (rr), maxon-maxon (mm), and maxon-roton (mr) states, respectively. The contribution of these states to $S(k, \omega)$ is proportional to the product of the DOS and the matrix element a .

The solid curve in Fig. 6 shows the calculated $S(k, \omega)$ for $k = 0.825 \text{ \AA}^{-1}$. The two-quasiparticle contribution has various peaks. The main peak occurs at $\omega \approx 25 \text{ K}$ and it is due to a one-maxon plus one-roton contribution. Two other peaks, one at $\omega \approx 20 \text{ K}$ and the other at $\omega \approx 28.5 \text{ K}$, are due to roton-roton and maxon-maxon contributions, respectively. Those three peaks come in our calculation at somewhat higher energies from the ones that can be found by summing the corresponding one-quasiparticle energies, because our two-quasiparticle propagator (2.38) has the pole at the solution of the following equation:

$$e_B(l) + \Sigma_0(l, \omega - e_B(m)) + e_B(m) + \Sigma_0(m, \omega - e_B(l)) = \omega. \quad (3.5)$$

The solutions of the above equation for l, m being the roton-roton, maxon-maxon, and maxon-roton momenta are systematically higher than $e(l) + e(m)$. We note that in principle the maxon-roton peak in $S(k, \omega)$ should be singular. However, in the results of numerical calculations shown in the figures it is not singular, due to crude resolution of numerical methods discussed in the Appendix.

At $k = 1.125 \text{ \AA}^{-1}$ the maxon-roton peak dominates the two-quasiparticle contribution to $S(k = 1.125, \omega)$ (Fig. 7). In $S(k = 1.525, \omega)$ (Fig. 8) the maxon-roton and roton-roton peaks are of comparable strengths, while at $k = 1.925 \text{ \AA}^{-1}$ there is no maxon-roton peak in the $S(k = 1.925, \omega)$ (Fig. 9), but there is a strong maxon-maxon and a relatively weaker roton-roton peak.

We can understand these changes from the behavior of

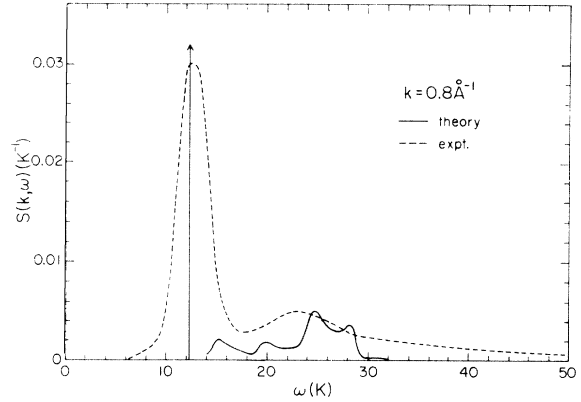


FIG. 13. The calculated $S(k, \omega)$ (solid line) is compared with the experimental data (dashed line) at $k = 0.8 \text{ \AA}^{-1}$.

the $a(k, l, m)$ and the DOS. In the neighborhood of $k \sim 1 \text{ \AA}^{-1}$ the matrix elements a_{rr} , a_{mm} , and a_{mr} have comparable magnitudes and so, as a result of the structure of the DOS (Fig. 11), the peak with higher intensity in $S(k, \omega)$ is the maxon-roton. For $k \sim 1.5 \text{ \AA}^{-1}$ the matrix element $|a_{rr}|$ is approximately twice as large as the $|a_{mr}|$ and $|a_{mm}|$ and so the roton-roton peak has comparable intensity with the maxon-roton peak even though it is not there in the DOS. At $k \sim 1.9 - 2.0 \text{ \AA}^{-1}$ the a_{mr} is very small, while the a_{rr} is significant and the a_{mm} is very big.

The $S(k = 0.825 \text{ \AA}^{-1}, \omega)$ has another peak at $\omega \approx 15 \text{ K}$. This is due to two-phonon states which are in the neighborhood of $\omega \approx ck$. The multiple-peak structure around 16–18 K of $S(k = 1.525, \omega)$ is presumably due to roton-phonon and maxon-phonon states.

In Fig. 13 we compare the calculated $S(k = 0.825, \omega)$ with the experimental⁵ $S(k, \omega)$ at $k = 0.8 \text{ \AA}^{-1}$. The lowest peak of the experimental $S(k, \omega)$ has to have zero width, but it is broadened by the instrumental resolution. In fact, the experimental resolution is essentially given by the width of this peak. The measured $S(k = 0.8, \omega)$ has a second broader and much weaker peak in the two-quasiparticle energy region at $\omega \approx 23 \text{ K}$, and a high-energy tail. The theoretical $S(k, \omega)$ has more structure in the two-quasiparticle energy region and the main peak is at the maxon-roton frequency $\omega \approx 25 \text{ K}$. A much better instrumental resolution is necessary to see this structure in experiments. A crude numerical broadening of the theoretical $S(0.825, \omega)$ with the present experimental resolution removes most of the structure. The theoretical two-quasiparticle peaks appear at somewhat higher ω (8–9% higher). This disagreement may be removed by the inclusion of self-energy corrections which involve four-FC-quasiparticle states. The inclusion of these states make the numerical calculation much more complicated and we leave them out in this work. The high-energy tail of the observed $S(k, \omega)$ is presumably due to three and more quasiparticle excitations omitted in this study.

C. The “quasifree” peak

In a neutron scattering experiment, if the momentum transfer k is very high, the neutron “sees” the individual helium atoms distributed with the microscopic momen-

tum distribution $n(p)$. In this case the dynamic structure factor may be approximated by the impulse approximation (IA)

$$S_{\text{IA}}(k, \omega) = \int \frac{d^3p}{(2\pi)^3 \rho} n(p) \delta \left[\omega - \frac{k^2}{2m} - \frac{\mathbf{p} \cdot \mathbf{k}}{m} \right], \quad (3.6)$$

where $n(p)$ is normalized as

$$\int \frac{d^3p}{(2\pi)^3 \rho} n(p) = 1. \quad (3.7)$$

The structure of $n(p)$ is as follows:

$$n(p) = n_c N \delta_{p,0} + n(p \neq 0), \quad (3.8)$$

where n_c is the condensate fraction of particles. In Ref. 12 we calculated $n(p)$ using the variational ground-state wave function. Now we can use the $n(p)$ and (3.6) to calculate $S_{\text{IA}}(k, \omega)$ and compare the results with the calculated $S(k, \omega)$ for high k . We obtain

$$S_{\text{IA}}(k, \omega) = n_c \delta \left[\omega - \frac{k^2}{2m} \right] + \frac{m}{4\pi^2 \rho} \frac{1}{k} \int_{P_{\min}}^{\infty} dp p n(p \neq 0), \quad (3.9)$$

$$P_{\min} = \left| \frac{k}{2} - \frac{m\omega}{k} \right|. \quad (3.10)$$

The second part of Eq. (3.9) peaks when $P_{\min} = 0$, i.e., at $\hbar^2 k^2 / 2m$ ($\equiv \omega_{\text{QF}}$). The first term is a δ -function peak also at $\omega = \omega_{\text{QF}}$. Its strength equals the fraction n_c of the particles in the $p=0$ condensate.

The impulse approximation is expected to be valid for very high k . Its validity has been criticized¹³ for hard-core liquids.

Before we compare our results for high k , at which the dominant peak of $S(k, \omega)$ is the "quasifree," we discuss the calculated $S(k, \omega)$ starting from the value of k where a peak appears in the neighborhood of $\hbar^2 k^2 / 2m$, for the first time.

As we have already discussed, in the interval $2.2 \text{ \AA}^{-1} \leq k \leq 2.7 \text{ \AA}^{-1}$ the strength of the one-quasiparticle peak is decreasing rapidly, and this is a signal that another peak has to appear elsewhere to compensate for the rest of the strength $S(k) - Z(k)$. In fact, this is the case in prac-

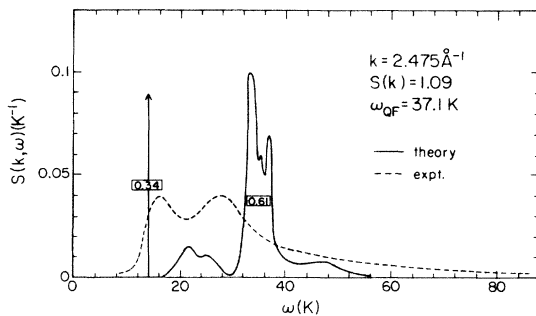


FIG. 14. The calculated $S(k, \omega)$ (solid line) is compared with the experiment (dashed line) at $k = 2.475 \text{ \AA}^{-1}$. The ω_{QF} given in top-right corner gives the quasifree scattering energy.

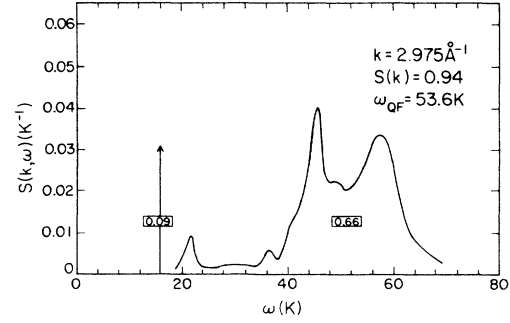


FIG. 15. The calculated $S(k = 2.975 \text{ \AA}^{-1}, \omega)$.

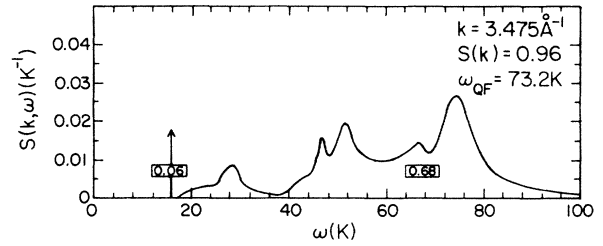


FIG. 16. The calculated $S(k = 3.475 \text{ \AA}^{-1}, \omega)$.

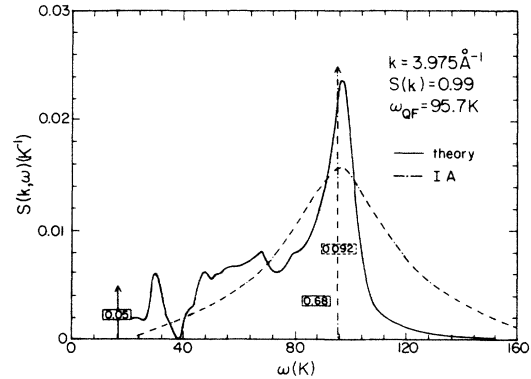


FIG. 17. The calculated $S(k = 3.975 \text{ \AA}^{-1}, \omega)$ (solid line) is compared with the results of the impulse approximation (dashed-dotted line).

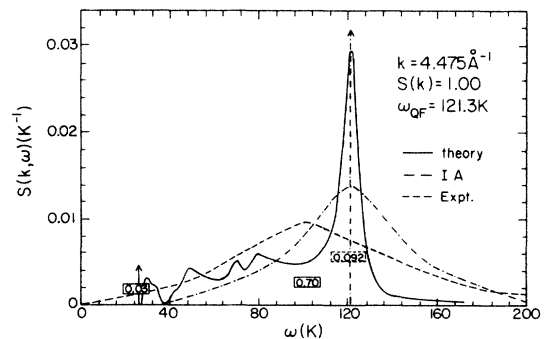


FIG. 18. The calculated $S(k, \omega)$ (solid line) is compared with the results of impulse approximation (dashed-dotted line) and the neutron-scattering data (dashed line) at $k = 4.475 \text{ \AA}^{-1}$.

TABLE I. Comparison of the calculated moments to $I_0(k) = \int d\omega S(k, \omega)$, $I_1(k) = \int d\omega \omega S(k, \omega)$ of $S(k, \omega)$ with exact ones: $S(k)$ and $\hbar^2 k^2/2m$, respectively. The columns $Z(k)$ and $Z(k)e(k)$ give contributions of the one-quasiparticle states to I_0 and I_1 , respectively.

k (\AA^{-1})	$Z(k)$	$I_0(k)$	$S(k)$	$Z(k)e(k)$ (K)	$I_1(k)$ (K)	$\hbar^2 k^2/2m$ (K)
0.825	0.14	0.17	0.21	1.73	2.51	4.12
1.125	0.19	0.25	0.31	2.55	4.05	7.67
1.525	0.41	0.53	0.60	4.72	7.50	14.1
1.925	1.09	1.25	1.35	9.7	13.6	22.5
2.475	0.35	0.96	1.09	4.8	26.0	37.1
2.975	0.09	0.75	0.94	1.4	34.6	53.6
3.475	0.06	0.74	0.96	0.96	44.5	73.2
3.975	0.05	0.73	0.99	0.90	55.1	95.7
4.475	0.03	0.71	1.00	0.77	68.7	121.3

tice. The calculated $S(k=2.475, \omega)$ shown in Fig. 14 has two main peaks. A δ -function peak at the energy $\omega \simeq 14$ K and strength $Z=0.34$, and a broad peak with some structure in the region of $\omega_{\text{QF}}=37$ K. In Figs. 14 to 18 the value of ω_{QF} is given in the top-right corner. The dashed line in Fig. 14 gives the experimental $S(k=2.5, \omega)$ taken from Fig. 6 of Ref. 1 and normalized in order to satisfy the sum rule (3.1). The two peak structure is present also in the experimental data. The theoretical and experimental strength of the peaks agree to a reasonable accuracy. The energies of the peaks of the calculated $S(k=2.475, \omega)$ appear at somewhat different energies from those of the experimental peaks.

The calculated $S(k, \omega)$ at $k=2.975$ and 3.475 \AA^{-1} (Figs. 15 and 16) has broad structures in the region of $\omega = \omega_{\text{QF}}$. These contain most of the strength. However, there are one or two significant peaks at lower ω . The contribution of the "one-quasiparticle" excitation has become insignificant.

The calculated $S(k=3.975 \text{ \AA}^{-1}, \omega)$ and $S(k=4.475 \text{ \AA}^{-1}, \omega)$ are compared with the impulse-approximation results in Figs. 17 and 18. The $S_{\text{IA}}(k, \omega)$ (dashed-dotted line) has a δ -function peak at $\hbar^2 k^2/2m$ with strength n_c

and another broad peak at the same place. In $S(k, \omega)$ (solid line) we find a sharp peak at $\hbar^2 k^2/2m$ and a broad structure in the neighborhood of this peak and at lower energies. The dashed curve in Fig. 18 shows the experimental $S(k, \omega)$ taken from Ref. 11. This curve has a broad peak at a lower value of $\omega \simeq 100$ K. Therefore the experimental data must have a very long energy tail in order to obtain an average energy $\omega = 121$ K required from the sum rule (3.2). It appears that $k=4.5 \text{ \AA}^{-1}$ is still low for the impulse approximation to be valid.

In Table I we give the calculated values of $Z(k)$ and the total integral $I_0(k)$ of the calculated $S(k, \omega)$ to be compared with $S(k)$. We also give the one-quasiparticle contribution to the sum rule (3.2) and $I_1(k) = \int d\omega \omega S(k, \omega)$ to be compared with $\hbar^2 k^2/2m$. We find that the sum rule (3.1) is violated by 7–29% and the sum rule (3.2) by 30–47%. To correct for this presumably one needs to consider higher contributions in the $S(k, \omega)$. Some of the neglected vertices and terms are given in Figs. 19(a)–19(d). Their contributions become more and more important as one tries to satisfy higher ω moments of $S(k, \omega)$. In the spirit of this theory the next terms to be included should be those with three-phonon states.

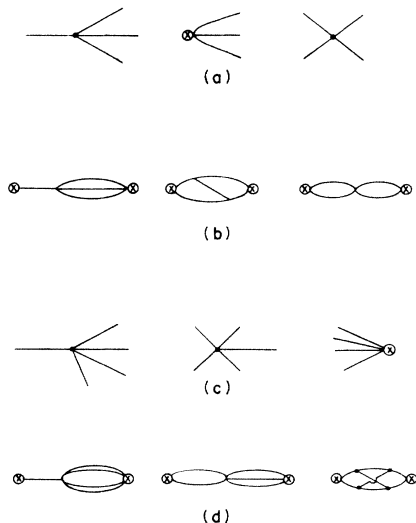


FIG. 19. Some of the neglected vertices and terms that contribute to the $D(k, \omega)$ and $S(k, \omega)$.

TABLE II. The numerically calculated two-particle density of states, using Eq. (4.2), for $k=0.885 \text{ \AA}^{-1}$ and $\omega=20$ K, as a function of ϵ and h .

ϵ (K)	h (\AA^{-1})	$\rho_2(k, \omega)$
2.0	0.05	0.399
2.0	0.025	0.339
2.0	0.0125	0.339
1.0	0.05	0.328
1.0	0.025	0.328
1.0	0.0125	0.328
0.4	0.05	0.319
0.4	0.025	0.323
0.4	0.0125	0.322
0.2	0.05	0.317
0.2	0.025	0.330
0.2	0.0125	0.322
0.2	0.00625	0.322

The new vertices at this level are shown in Fig. 19(a) and some of the new $D(k, \omega)$ contributions are illustrated in Fig. 19(b). The still higher level of accuracy should include four-phonon states illustrated in Figs. 19(c) and 19(d). Hopefully the contribution of the various diagrams to $S(k, \omega)$ decreases rapidly as the number of interacting phonons increases. Nevertheless, the present calculation with only one- and two-phonon states seems to give a

semiquantitative description of the $S(k, \omega)$ over a wide range of k and ω .

ACKNOWLEDGMENTS

The authors wish to thank Professor David Pines and Dr. W. Stirling for many valuable discussions. This work was supported by the U.S. Department of Energy, Division of Materials Sciences under Contract No. DE-AC02-76ER01198.

APPENDIX

1. Calculation of the density of states

The two-quasiparticle DOS is defined by Eq. (3.3). If we consider the following representation of the δ function:

$$\delta_\epsilon(x) = \frac{1}{\sqrt{\pi\epsilon}} e^{-(x/\epsilon)^2}, \quad (\text{A1})$$

where $\delta(x)$ is the limit of the above distribution for $\epsilon \rightarrow 0$, the DOS may be written as

$$\rho_2(k, \omega) = \lim_{\epsilon \rightarrow 0} \left[\frac{1}{8\pi^2 \rho k} \int dl l \int_{|k-l|}^{k+l} dm m \delta_\epsilon(\omega - e(l) - e(m)) \right]. \quad (\text{A2})$$

In practice we calculate ρ_2 at a chosen value of ϵ and test the convergence of the $\lim_{\epsilon \rightarrow 0}$ by recalculating the ρ_2 with an ϵ that is smaller by approximately a factor of 2. The numerical integral is calculated with a grid spacing h for the l and m mesh. As ϵ is reduced, it is necessary to decrease h to assure accuracy of the numerical methods. The limit $\epsilon \rightarrow 0$ is achieved when the results are stable with respect to variations in ϵ and the grid spacing h of the integration. The results of the integral (A2) for $k=0.885 \text{ \AA}^{-1}$ and $\omega=20 \text{ K}$ are shown in Table II. We notice that the convergence is achieved for $\epsilon \simeq 0.4 \text{ K}$ and $h=0.025 \text{ \AA}^{-1}$.

Another representation of the δ function may be the following:

$$\delta_\epsilon(x) = \frac{1}{\pi} \frac{\epsilon}{\epsilon^2 + x^2}. \quad (\text{A3})$$

A calculation of $\rho_2(k, \omega)$ with the representation (A3) shows that the convergence is much slower and the required values of ϵ and h are smaller. Therefore, the form (A1) is more convenient for practical reasons.

2. Calculation of $\Sigma_0(k, \omega)$

From Eqs. (2.20) and (2.32)–(2.33) we may write

$$\Sigma_0(k, \omega) = \text{Re}[\Sigma_0(k, \omega)] + i \text{Im}[\Sigma_0(k, \omega)], \quad (\text{A4})$$

$$\text{Im}[\Sigma_0(k, \omega)] = -\frac{\pi}{2} \sum_{l, m} |a(k, l, m)|^2 \delta(\omega - e_B(l) - e_B(m)), \quad (\text{A5})$$

$$\text{Re}[\Sigma_0(k, \omega)] = \frac{1}{\pi} \int_0^\infty d\omega' \frac{\text{Im}[\Sigma_0(k, \omega')]}{\omega' - \omega}. \quad (\text{A6})$$

We calculate the $\text{Im}[\Sigma_0(k, \omega)]$ using the expression

$$\text{Im}[\Sigma_0(k, \omega)] = -\frac{1}{8\pi^2 \rho k} \int_0^\infty dl l \int_{|k-l|}^{k+l} dm m |a(k, l, m)|^2 \delta_\epsilon(\omega - e_B(l) - e_B(m)), \quad (\text{A7})$$

where $\delta_\epsilon(x)$ is the representation (A1) and $\epsilon=0.4 \text{ K}$.

The real part of $\Sigma_0(k, \omega)$ may be written as

$$\text{Re}[\Sigma_0(k, \omega)] = -\frac{1}{2} \sum_{l, m} \frac{|a(k, l, m)|^2}{e_B(l) + e_B(m) - \omega} \Theta(|e_B(l) + e_B(m) - \omega| - \eta) + \frac{1}{\pi} \int_{|\omega' - \omega| < \eta} d\omega' \frac{\text{Im}[\Sigma_0(k, \omega')]}{\omega' - \omega}. \quad (\text{A8})$$

For small η the second term is approximated by

$$\frac{1}{\pi} 2\eta \frac{\partial \text{Im}[\Sigma_0(k, \omega)]}{\partial \omega}. \quad (\text{A9})$$

The value $\eta=0.4 \text{ K}$ is used in the calculations. The contribution of the second term of Eq. (A8) is very small for this value of η , and we have verified that the results do not change when η is reduced to 0.2 K .

3. Calculation of $\Sigma(k, \omega)$

The real and imaginary parts of $\Sigma(k, \omega)$ are given as follows:

$$\begin{cases} \text{Re}[\Sigma(k, \omega)] \\ \text{Im}[\Sigma(k, \omega)] \end{cases} = -\frac{1}{8\pi^2 \rho k} \int_0^\infty dl l \int_{|k-l|}^{k+l} dm m |a(k, l, m)|^2 \begin{cases} \times \text{Re}[G_2(l, m, \omega)] , \\ \times \text{Im}[G_2(l, m, \omega)] , \end{cases} \quad (\text{A10})$$

where if $\Gamma_2(l, m, \omega)$ [Eq. (2.45)] is greater than ϵ , the $\text{Re}[G_2(l, m, \omega)]$ and $\text{Im}[G_2(l, m, \omega)]$ are given by Eqs. (2.42) and (2.43). If $\Gamma_2(l, m, \omega)$ is less than ϵ we use Eqs. (2.46) and (2.47) for the real and imaginary part of $G_2(l, m, \omega)$. The following representations are used for the principal values and δ function:

$$\text{Re}[G_2(l, m, \omega)] = \frac{1}{e_2(l, m, \omega) - \omega} \left\{ 1 - \exp \left[- \left[\frac{e_2(l, m, \omega) - \omega}{\epsilon} \right]^2 \right] \right\}, \quad (\text{A11})$$

$$\text{Im}[G_2(l, m, \omega)] = \pi \left\{ \frac{1}{\sqrt{\pi \epsilon}} \exp \left[- \left[\frac{e_2(l, m, \omega) - \omega}{\epsilon} \right]^2 \right] \right\}. \quad (\text{A12})$$

We use the value of $\epsilon = 0.2$ K for calculating $\Sigma(k, \omega)$, and the integrals over l and m are done with grid spacing $h = 0.0125 \text{ \AA}^{-1}$. The integrals $\zeta(k, \omega)$ and $D'(k, \omega)$ [Eqs. (2.40) and (2.41)] are also evaluated in a similar fashion.

¹See, for review, A. D. B. Woods and R. A. Cowley, Rep. Prog. Phys. **36**, 1135 (1973).

²E. Manousakis and V. R. Pandharipande, Phys. Rev. B **30**, 5062 (1984).

³T. J. Greytak and J. Yan, Phys. Rev. Lett. **22**, 987 (1969); T. J. Greytak, R. Woerner, J. Yan, and R. Benjamin, *ibid.* **25**, 1547 (1970).

⁴A. Zawadowski, J. Ruvalds, and J. Solana, Phys. Rev. A **5**, 399 (1972).

⁵E. C. Svensson, P. Martel, V. F. Sears, and A. D. B. Woods, Can. J. Phys. **54**, 1976.

⁶R. Hasting and J. W. Halley, Phys. Rev. A **10**, 2488 (1974).

⁷H. W. Jackson, Phys. Rev. A **8**, 1529 (1973).

⁸D. Pines in Proceedings of the Third International Conference on Recent Progress in Many-Body Theories, Altenberg, West Germany, 1983 (unpublished).

⁹R. P. Feynman and M. Cohen, Phys. Rev. **102**, 1186 (1956).

¹⁰A. L. Fetter and J. D. Walecka, *Quantum Theory of Many-Particle Systems* (McGraw-Hill, New York, 1971).

¹¹R. A. Cawley and A. D. B. Woods, Can. J. Phys. **49**, 177 (1971).

¹²E. Manousakis, V. R. Pandharipande, and Q. N. Usmani, Phys. Rev. B **31**, 7022 (1985).

¹³J. J. Weinstein and J. W. Negele, Phys. Rev. Lett. **49**, 1016 (1982).